Impact of MODIS and AIRS total precipitable water on modifying the vertical shear and Hurricane Emily simulations

Yi-Chin Liu,[1] Shu-Hua Chen,[1] and Fang-Ching Chien[2]

Received 25 May 2010; revised 2 November 2010; accepted 2 December 2010; published 28 January 2011.

[1] The impact of retrieved total precipitable water (TPW) from Moderate Resolution Imaging Spectrometer (MODIS) infrared (IR), MODIS near-infrared (NIR), and the combined Atmospheric Infrared Sounder (AIRS)-IR and Advanced Microwave Sounding Unit-Microwave channels on simulations of Hurricane Emily was assessed and compared using the Weather Research and Forecasting model and its three-dimensional variation data assimilation (3D-Var) system. After assimilating MODIS IR TPW, the model clearly better reproduced storm tracking, intensity, and the 10 m wind field, while the improvement was limited or nil when assimilating either MODIS NIR TPW or AIRS TPW. After the data assimilation of MODIS IR TPW, a positive moisture increment was present to the east of the simulated storm in 3D-Var analysis (i.e., initial conditions). The positive TPW increment enhanced a convective cloud, which was also observed by satellites. The convective cloud effectively modulated the height and wind fields, resulting in a weakening of the vertical wind shear (VWS) over the region. The weak VWS band was then advected to the north of the storm, preventing the storm from attaching to the strong VWS zone located between 20°N and 30°N. There was no such positive moisture increment, convective cloud, or weak VWS band occurring to the east of the simulated storm in the other data assimilation experiments. This explains why the simulated storm intensified with assimilation of MODIS IR TPW but not for the other experiments.

Citation: Liu, Y.-C., S.-H. Chen, and F.-C. Chien (2011), Impact of MODIS and AIRS total precipitable water on modifying the vertical shear and Hurricane Emily simulations, *J. Geophys. Res.*, *116*, D02126, doi:10.1029/2010JD014528.

1. Introduction

[2] Numerical weather prediction is an initial and boundary value problem [*Kalnay*, 2003]. Therefore a more accurate estimate of the initial conditions should theoretically result in better forecasts and simulations. Thus uncertainties in the moisture and the absence of important mesoscale features over oceanic areas are primary concerns for an initial state of tropical cyclone (TC) forecasts and simulations. Fortunately, over the past two decades, considerable progress has been made in satellite technology and has significantly contributed a vast amount of information in data-sparse areas. With proper and effective assimilation of satellite data, it has become possible to obtain improved initial conditions and thus better TC forecasts and simulations.

[3] Moderate Resolution Imaging Spectrometer (MODIS) and Atmospheric Infrared Sounder (AIRS) are two novel instruments on satellites that monitor atmospheric moisture. MODIS instruments, which are on board the NASA Earth Observation System Terra and Aqua satellites, have channels in two regions of the electromagnetic spectrum that observe atmospheric moisture and temperature: near-infrared (NIR) and infrared (IR). The resolutions of the level 2 total precipitable water (TPW) retrieved from NIR and IR algorithms are 1 and 5 km, respectively. Such a high spatial resolution makes MODIS a good instrument to describe detailed horizontal gradients of moisture and temperature. AIRS and its companion, Advanced Microwave Sounding Unit (AMSU), are also on board the Aqua satellite. The AIRS standard level 2 products are retrieved from the combined AIRS-IR and AMSU-microwave (MW) channels. AIRS uses high-spectral-resolution true sounder radiance, which is capable of providing near-radiosonde-quality vertical profiles of atmospheric temperature and moisture. TPW is an AIRS standard level 2 product with a resolution of 45 km.

[4] The accuracy of satellite retrievals (e.g., TPW) can be influenced by uncertainties of the instruments and spectral calibrations, by assumptions of retrieval algorithms, and, in some cases, by cloud contamination in the field of view [*Seemann et al.*, 2003; *Strow et al.*, 2006]. To understand the error characteristics associated with these retrievals, many validation studies have been conducted [*Kleidman et al.*, 2000; *Gao and Kaufman*, 2003; *Seemann et al.*, 2003; *Zhang et al.*, 2007; *Chen et al.*, 2008]. *Kleidman et al.* [2000]

[1]Department of Land, Air, and Water Resources, University of California, Davis, California, USA.
[2]Department of Earth Sciences, National Taiwan Normal University, Taipei, Taiwan.

0148-0227/11/2010JD014528

showed that the root-mean-square error (RMSE) of MODIS NIR TPW over ocean is about 5.0 mm and the magnitude of TPW is likely an underestimate in a dry atmosphere. *Chen et al.* [2008] demonstrated that the RMSE of MODIS NIR TPW is about 3.3 mm over land. TPW is slightly underestimated by less than 1 mm in a dry atmosphere and overestimated by up to 7 mm in a moist atmosphere. In contrast, MODIS IR TPW over land is overestimated (underestimated) in a dry (moist) atmosphere, with the maximum deviation of up to 5 mm and an RMSE of 4.1 to 5.2 mm [*Seemann et al.*, 2003; *Chen et al.*, 2008]. *Rama Varma Raja et al.* [2008] compared AIRS TPW with derived TPW from a network of ground-based global positioning systems over the United States and found that the bias and RMSE are 1.2 and 4.14 mm in the summer and −0.5 and 3 mm in the winter, respectively. They also suggested that AIRS TPW tends to be underestimated (overestimated) in a moist (dry) atmosphere.

[5] Unlike validation studies, relatively little research has been conducted regarding the assimilation of MODIS and AIRS TPW. *Chen et al.* [2008] assimilated MODIS NIR TPW for a thunderstorm case and Hurricane Isidore (2002) and showed that the rainfall distribution of the thunderstorm and the intensity of Isidore were greatly improved.

[6] The evolution of TCs can be influenced by vertical wind shear (VWS), sea surface temperature, sea surface moisture flux, upper tropospheric eddy-relative angular momentum flux convergence, and tropospheric water vapor flux [*Frank*, 1977], with VWS as one of the most important environmental variables that controls TC development [*Aiyyer and Thorncroft*, 2006; *Black et al.*, 2002; *Bracken and Bosart*, 2000; *DeMaria*, 1996; *Frank and Ritchie*, 2001; *Gray*, 1968; *Jones*, 2000; *Wang and Holland*, 1996; *Zehr*, 1992; *Zhu et al.*, 2004]. For example, *Aiyyer and Thorncroft* [2006] used 46 years of European Centre for Medium-Range Weather Forecasts 40 year reanalysis data to examine the impact of VWS on TC activity over the main development region (7.5°–20°N, 85°–15°W) in the Atlantic Ocean basin. They found that VWS accounts for almost 50% of TC activity within this region. In general, the impact of VWS on TC formation and intensity is negative.

[7] Hurricane Emily (2005), the case studied in this paper, has also been studied previously [*Li and Pu*, 2008, 2009; *Pu et al.*, 2009; *Cecil et al.*, 2010]. Emily first formed over the central tropical Atlantic on the evening of 10 July 2005 and rapidly developed into a hurricane on July 13. It then went through two rapid intensification periods, and on 17 July 2005 it became the most intense hurricane that was ever recorded over the Atlantic Ocean in the month of July [*Beven et al.*, 2008] (see also J. L. Franklin and D. P. Brown, Tropical cyclone report: Hurricane Emily, 11–21 July 2005, at http://www.nhc.noaa.gov/pdf/TCR-AL052005_Emily.pdf). *Li and Pu* [2008] proposed that Emily's first rapid intensification was influenced by the distribution of eye wall convective heating and the latent heat flux from the ocean surface. In a later study, *Pu et al.* [2009] used the Weather Research and Forecasting (WRF) model with different spatial resolutions (3 and 1 km) and initial conditions (with and without data assimilation) to diagnose factors that had a large influence on Emily's first rapid intensification. The assimilation of satellite data improved the simulated storm's intensity, but increases in resolution (i.e., 3 to 1 km) had little impact.

[8] The primary objectives of this study are to evaluate the impact of assimilating MODIS and AIRS TPW on Emily simulations and to examine the influence of the VWS changes on the simulated hurricane intensity. Because both MODIS and AIRS instruments are on board the Aqua satellite, they provide a great opportunity to study the impact of assimilating different data on the same storm simulations. This paper is organized as follows. The intercomparison of TPW data sets from MODIS and AIRS is presented in section 2. The numerical modeling system, including the WRF model and its variational data assimilation component, and the experiment design are described in section 3. Numerical simulation results and three sensitivity studies are discussed in section 4 along with concluding remarks at the end.

2. Data Intercomparisons

[9] As discussed above, data comparison studies have estimated the possible observational error range associated with the three TPW data sets (i.e., MODIS IR, MODIS NIR, and AIRS). However, most of them were analyzed over land because of limited conventional sounding data available over ocean. Thus the observational errors for TPW over ocean are undetermined. Here these three data sets were intercompared over land and ocean to understand their relative data characteristics (i.e., which one is drier or moister) over both land and ocean, which can help explain the different simulation results associated with those data. TPW data over the Atlantic and Pacific oceans, North America, and East Asia during September 2002 and July–September 2005 were used. As a result of the different resolutions of these data sets (i.e., 1 km for MODIS NIR, 5 km for MODIS IR, and 45 km for AIRS), for each pairwise comparison the higher-resolution data were downscaled to the pixel size of the low-resolution counterpart.

[10] Results showed that over land, TPW data from all three instruments were comparable, but with some notable differences (Figures 1a, 1c, and 1e). TPW from MODIS IR was slightly moister (drier) than MODIS NIR in a relatively dry (moist) environment (Figure 1a), consistent with published bias characteristics [*Chen et al.*, 2008; *Gao and Kaufman*, 2003]. TPW from both MODIS NIR and MODIS IR was consistently slightly moister than AIRS. Thus, over land, AIRS TPW was statistically the driest (Figures 1c and 1e). Results in a moist environment were consistent with those of *Chen et al.* [2008] and *Rama Varma Raja et al.* [2008], while those in a dry atmosphere were not. The inconsistency is likely because the dry bias for NIR and the moist bias for AIRS over land are relatively small in a dry atmosphere. Thus the results can be very sensitive to the number and locations of samples.

[11] Over ocean, MODIS NIR TPW was the driest in both dry and moist environments, and MODIS IR TPW was the moistest (Figures 1b, 1d, and 1f). This implies that the MODIS NIR TPW might have a dry bias over ocean, which agrees with *Kleidman et al.* [2000].

3. Methodology

[12] This section provides a brief description of the model configuration and setup, the experiment design, the quality

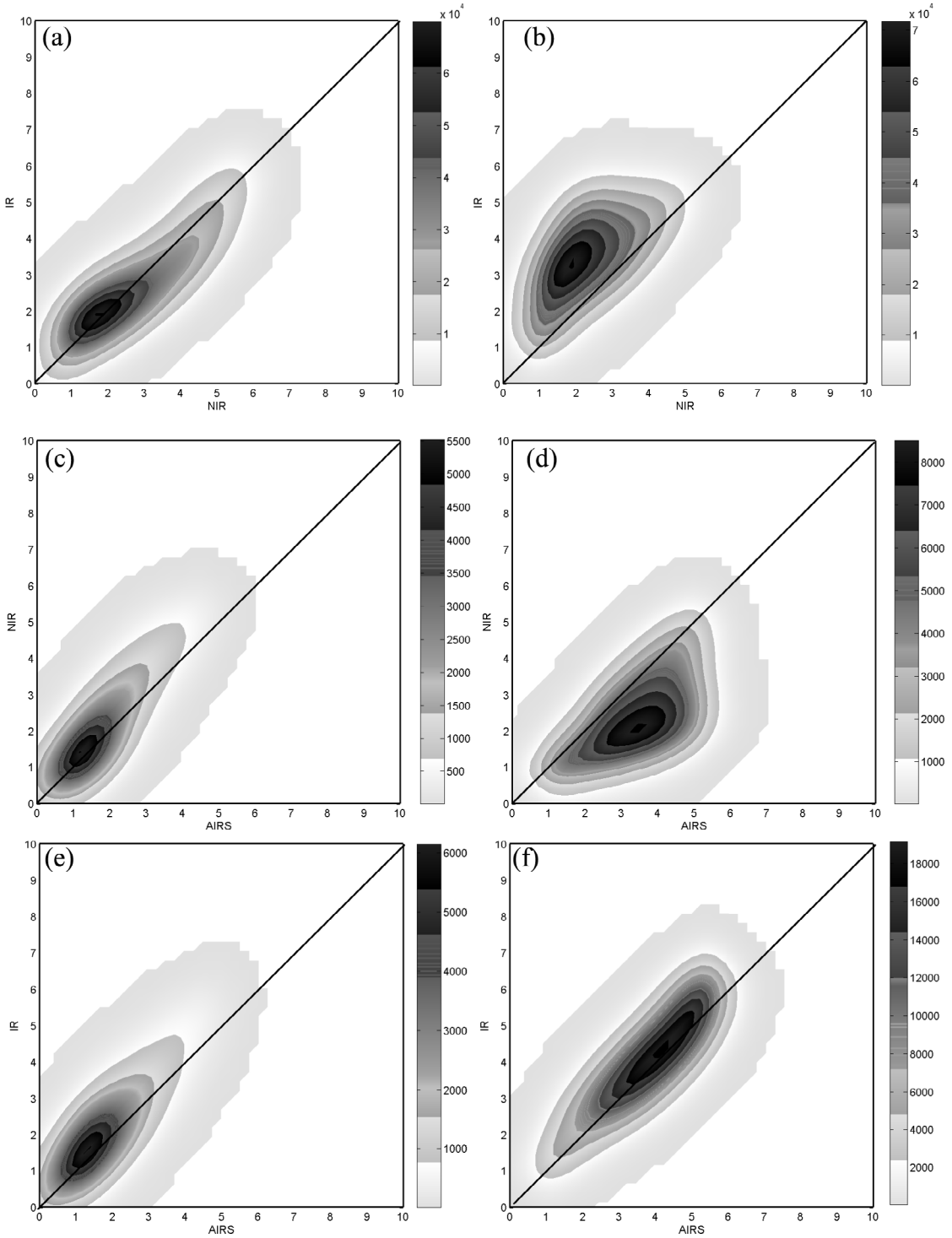

Figure 1. Point density plots (points/area) of the observed TPW (cm) for (a) MODIS NIR versus MODIS IR, (c) AIRS versus MODIS NIR, and (e) AIRS versus MODIS IR over land. (b, d, f) Same as Figures 1a, 1c, and 1e, respectively, except for over ocean.

control of the satellite-retrieved TPW, and the process of TPW data assimilation.

3.1. Model Settings and Experiment Design

[13] The Advanced Research WRF model version 2.1 and its three-dimensional variational data assimilation system (3D-Var) were used [*Skamarock et al.*, 2008]. The domain configuration included two two-way nested domains of 30 and 10 km horizontal resolutions. The grids extended vertically to 50 hPa and were resolved by 31 unevenly spaced sigma levels with the finest resolution in the boundary layer. The physics parameterization schemes that were applied to

Table 1. Numerical Experiment Designs for Simulations of Hurricane Emily[a]

Experiment	Data Assimilated
ENONE	none
EMN	MODIS NIR TPW
EMI	MODIS IR TPW
EG	GTS
EMNG	MODIS NIR TPW + GTS
EMIG	MODIS IR TPW + GTS
EA	AIRS TPW
EAG	AIRS TPW + GTS

[a]The first letter in experiment names, E, denotes Emily. "None" indicates that no observations were assimilated. The letter G denotes the assimilation of GTS data, which include conventional surface observations and radiosondes. MN is for Moderate Resolution Imaging Spectroradiometer (MODIS) near-infrared (NIR) total precipitable water (TPW), MI indicates MODIS infrared (IR) TPW, and A denotes Atmospheric Infrared Sounder (AIRS) TPW.

the simulations included the Purdue-Lin microphysics [*Chen and Sun*, 2002], the new Kain-Fritsch cumulus parameterization [*Kain*, 2004], the Yonsei University boundary layer parameterization [*Hong et al.*, 2006], the Dudhia shortwave parameterization [*Dudhia*, 1989], and the Rapid Radiative Transfer Model longwave parameterization [*Mlawer et al.*, 1997]. The initial and lateral boundary conditions and sea surface temperature data were from the National Centers for Environmental Prediction Global Forecast System (GFS) with spatial and temporal resolutions of 1° × 1° and 6 h, respectively. A data-screening process was performed hourly for 6 h, starting from 1200 UTC 13 July 2005. The model was then integrated for 72 h starting from 1800 UTC 13 July 2005. Since some observations have already been assimilated into the GFS analyses, the assimilation of observations started 1 h after the model integration in the 6 h cycling period.

[14] Table 1 shows the experiments and the corresponding observations that were assimilated in the 3D-Var procedures. The conventional observations (referred to as GTS hereinafter), which include surface station reports and radiosondes, were assimilated at every hour, whereas the assimilation of satellite data (i.e., MODIS IR, MODIS NIR, and AIRS TPW) was performed only when the data were available.

3.2. Data Quality Control

[15] For MODIS IR TPW, data over cloudy areas were excluded in the original data set. Therefore no more data screening was performed during the preprocessing stage. For MODIS NIR TPW, data over clear-sky and cloudy regions were available in the data set. Since the TPW data over the cloudy region is the vertical integral of water vapor only above the cloud top, in general, one prefers not to use those data in 3D-Var. In processing MODIS NIR TPW, the resolution of data was reduced from 1 to 5 km by averaging data from cloud-free pixels in 5 × 5 matrices, with a required minimum of 10 clear-sky pixels identified using the cloudiness flag provided in the data set. Consequently, many MODIS NIR TPW data near the cloudy area were discarded. As for the AIRS TPW, only those data with the best quality (i.e., quality indicator, Qual_H2O, is "best") were used. Since MV-channel data are not affected by clouds, except by heavy precipitation and the uncertainty in surface emissivity, AIRS can theoretically provide moisture information over cloudy areas, while MODIS IR and NIR TPW are unavailable over those regions.

[16] Following the gross-error quality control used for most of the observations in WRF 3D-Var, satellite TPW data that differed from the model's background by more than 5 times the observation-error variance were removed. An observation error of 4 mm was used for both MODIS and AIRS TPW data.

3.3. Data Assimilation of TPW

[17] The WRF 3D-Var system utilizes the incremental approach. The analysis state, $\mathbf{x}^a$, is obtained by

$$\mathbf{x}^a = \mathbf{x}^b + \delta\mathbf{x}^a, \tag{1}$$

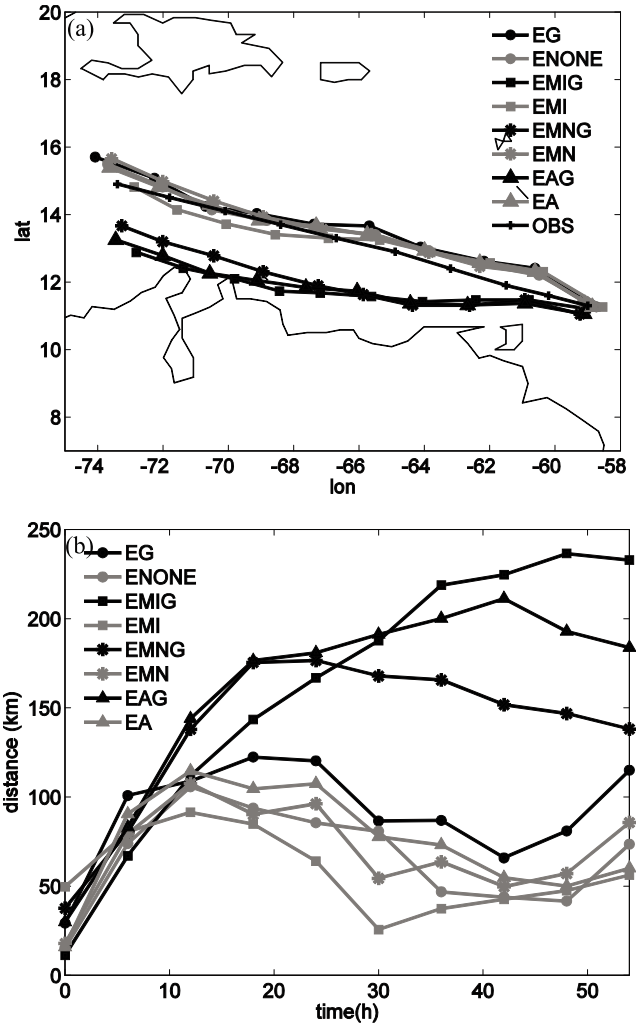

Figure 2. The (a) 54 h simulated tracks from 1800 UTC 13 July to 0000 UTC 16 July 2005 and (b) time evolution of simulated track errors (km), which were defined as the distance between the simulated storm's center and the best-track position.

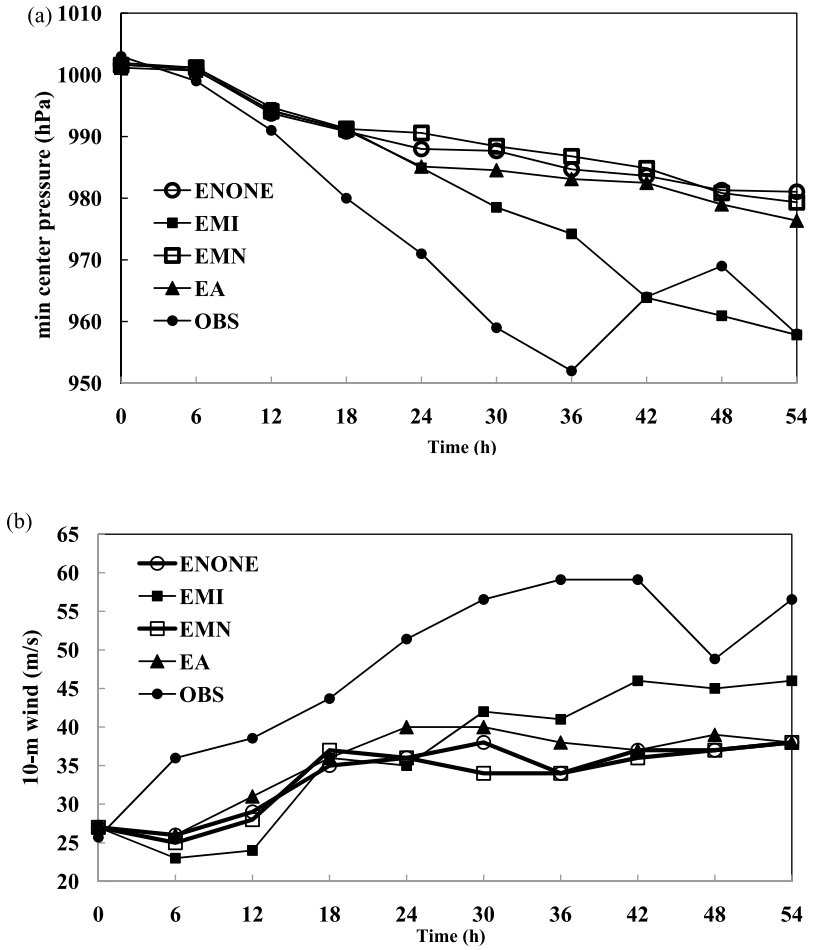

Figure 3. Time series of the observed and simulated (a) minimum central SLP (hPa) and (b) maximum 10 m wind speed (m s^{-1}) from the National Hurricane Center best-track data (OBS) and the numerical simulations during 1800 UTC 13 July to 0000 UTC 16 July 2005.

where $\mathbf{x}^b$ is the background state (i.e., the first guest) and $\delta\mathbf{x}^a$ is the analysis increment of TPW obtained by minimizing the following cost function (J):

$$J(\delta\mathbf{x}) = \frac{1}{2}\delta\mathbf{x}^T B^{-1}\delta\mathbf{x} + \frac{1}{2}\sum_{n=0}^{N}\{TPW_{model} - TPW_{obs}\}^T \cdot O^{-1}\{TPW_{model} - TPW_{obs}\}, \quad (2)$$

where B is the covariance matrix of background errors, O is the covariance matrix of observational errors, and N is the total number of available observations. TPW_{model} represents TPW from the background state that was computed using a forward operator in the 3D-Var system, and the formula is as follows:

$$TPW_{model} = \frac{p^*}{g}\sum_{k=1}^{KX} q(k)\Delta\sigma(k), \quad (3)$$

where p^* is defined as the difference in the pressure between the model surface and top, q(k) the model-specific humidity at the kth layer, $\Delta\sigma(k)$ is the layer thickness of the model at the kth layer, and KX is the total number of layers. After the minimization of the cost function, the adjoint TPW operator and the spatial correlations (from the background covariance matrix) project two-dimensional TPW increments onto 3-D moisture increments.

4. Discussion of the Results

[18] The performance of each simulation was evaluated by comparing with observations of TC track, minimum sea level pressure (SLP), maximum 10 m winds, and 10 m wind structure. The impact of assimilating TPW data from different instruments on Emily's simulations was then investigated.

4.1. Verification

[19] The observed (from the best track) and simulated tracks of Emily, which were defined by the minimum SLP, from 0 to 54 h integration, are shown in Figure 2. Only the first 54 h simulation is presented because the simulated hurricane moved out of domain 2 after 54 h. The observed Emily moved west northwestward during the simulation period. The simulated tracks of experiments EMNG, EMIG, and EAG, which assimilated both GTS and TPW data, were shifted to the south of the observed track. The track errors of

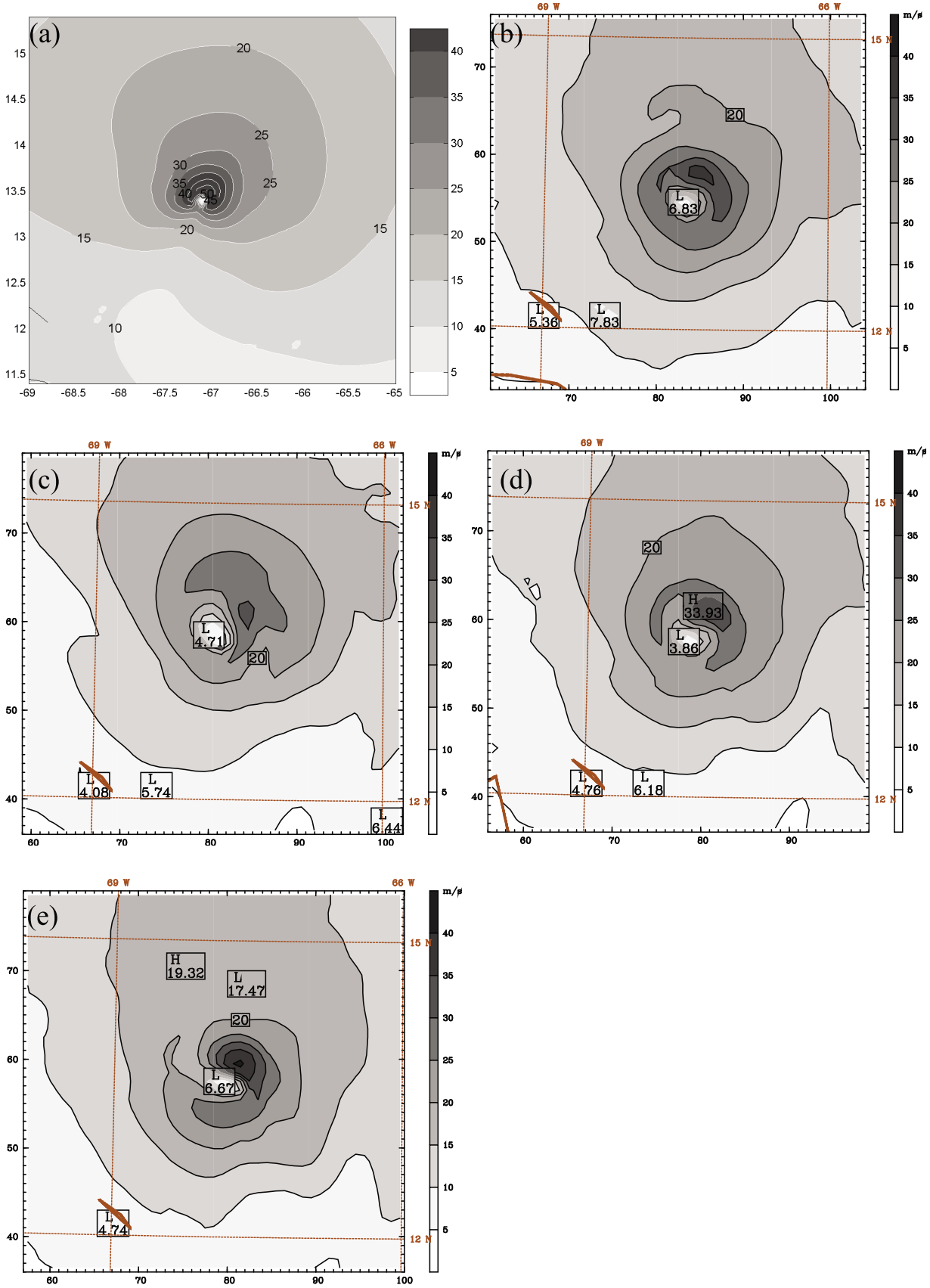

Figure 4. Ten meter wind speed (m s^{-1}) from the (a) NOAA Hurricane Research Division at 0130 UTC 15 July 2005 and from (b) EMI, (c) EMN, (d) EA, and (e) ENONE at 32 h (0200 UTC 15 July 2005).

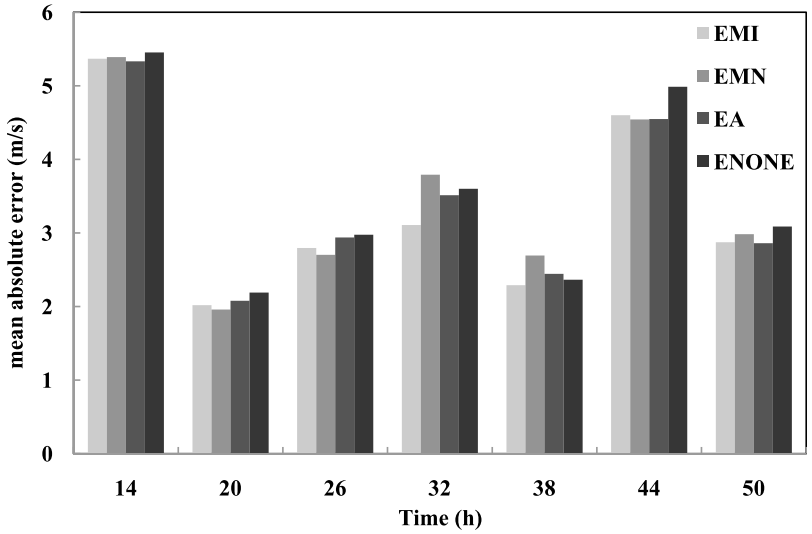

Figure 5. Mean absolute error of 10 m wind (m s^{-1}) averaged inside a 400 km × 400 km box following the hurricane center, computed from the difference between EMI, EMN, EA, and ENONE and the observations at 14, 20, 32, 38, 44, and 50 h.

these three experiments increased significantly after 12 h, exceeding 150 km, on average (Figure 2b). For the experiments in which only TPW data were assimilated (EMI, EMN, and EA), only GTS data were assimilated (EG), or no observations were assimilated (ENONE), the simulated tracks were very close to the observation, and the time-averaged track errors were less than 130 km. In particular, EMI produced the smallest track error.

[20] In general, the use of GTS data could statistically improve the simulation of the large-scale flow, which, consequently, results in better tracks. However, GTS data still contain observational errors. In some cases, if the quality of the background was better than that of the GTS data (e.g., simulated Emily's track was comparable to observation from ENONE in this study) or the GTS data were misinterpreted after 3D-Var because of inhomogeneity or sparseness of the data (i.e., producing unreasonable gradients of increments), simulated results could become worse. The experiments with GTS data in this study have probably fallen into this type of case. After the assimilation of both TPW and GTS data, a large area of northerly wind anomaly at low and high levels was present (data not shown). This caused the simulated tracks to deflect to the south of the observation. Since this study focuses on the impact of retrieved satellite data, examining the simulation results with incorrect track would complicate the discussion, and therefore the experiments with the data assimilation of GTS data are excluded in the later discussion.

[21] Figure 3a shows the time evolution of the storm's minimum SLP from the best track and the simulations (ENONE, EMI, EMN, and EA). The observed central SLP deepened from 1003 hPa at the model initial time (i.e., 1800 UTC 13 July 2005) to 953 hPa 36 h later. The central SLP of Emily increased later and then decreased slightly from 36 to 54 h, when Emily experienced an eye wall replacement. Without assimilating any observational data, ENONE produced a weaker storm with the minimum SLP about 15–30 hPa weaker than the observation throughout the simulation. Compared to ENONE, the simulated central SLP from EMI was significantly improved, although it was still weaker than observations. EA had slightly better simulated intensity than ENONE. With the use of MODIS NIR TPW, the simulated hurricane intensity from EMN was worse than that from ENONE. These four simulations all failed to capture the eye wall replacement process. Besides the potential deficiency of the WRF model and the model initial conditions, the coarse resolution could be another reason for such failure [*Nolan et al.*, 2009; *Gentry and Lackmann*, 2010]. A similar result was found in the comparison of maximum 10 m wind speed among the experiments (Figure 3b). The maximum 10 m wind of EMI was the closest to the observation, followed by EA, ENONE, and EMN.

[22] The observed 10 m winds were relatively asymmetric, with a maximum wind speed of 50 m s^{-1} to the north northeast at 0130 UTC 15 July (Figure 4a). This implies that VWS should exist in the environment because it is one of the main causes of asymmetric hurricane structures [*Miller*, 1958; *Burpee and Black*, 1989; *Franklin et al.*, 1993; *Marks et al.*, 1992]. Note that there was a 30 min difference

Table 2. The Statistical Significance Levels for EMI, EMN, and EA Under the Hypothesis That the Mean Absolute Error of the 10 m Winds for ENONE is Larger Than Those of EMI, EMN, and EA, respectively, at 14, 20, 26, 32, 38, 44, and 50 h[a]

Time (h)	EMI	EMN	EA
14	0.784	0.880	0.985
20	0.999	0.999	0.999
26	0.984	0.999	×[a]
32	0.999	×[a]	0.928
38	0.991	×[a]	×[a]
44	0.999	0.999	0.999
50	0.999	0.999	0.999

[a]The hypothesis was violated.

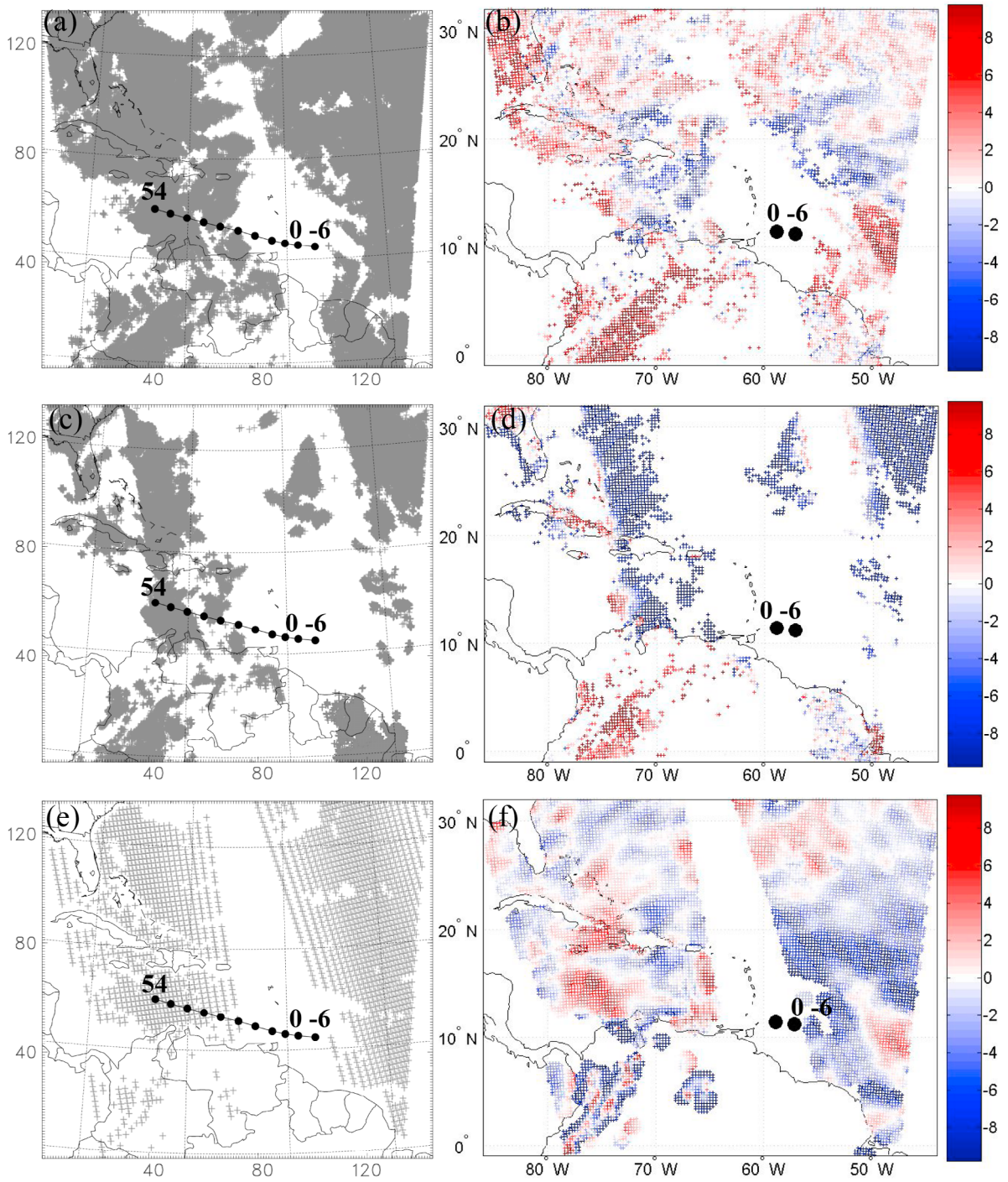

Figure 6. Coverage area of satellite data (gray plus) and the innovation (positive (negative) values are shaded in warm (cold) colors; mm) from (a and b) MODIS IR, (c and d) MODIS NIR, and (e and f) AIRS TPW, respectively, during the 6 h data update cycling period (1200 UTC 1800 UTC 13 July 2005). Black dots indicate Hurricane Emily's best track position during the 6 h update cycling (−6 to 0 h) and 54 h integration time period (0–54 h).

between observation and model simulation because model outputs were saved at every hour. Results show that ENONE, EMI, EMN, and EA reproduced reasonably well the structure and location of the asymmetric wind (Figures 4b–4e). However, the area where winds were larger than 25 m s^{-1} was smaller than in the observation because of the weaker simulated intensity. The maximum wind area of EMI (winds >25 m s^{-1}) was the largest among all experiments and the most consistent with the observation, followed by ENONE, EA, and EMN.

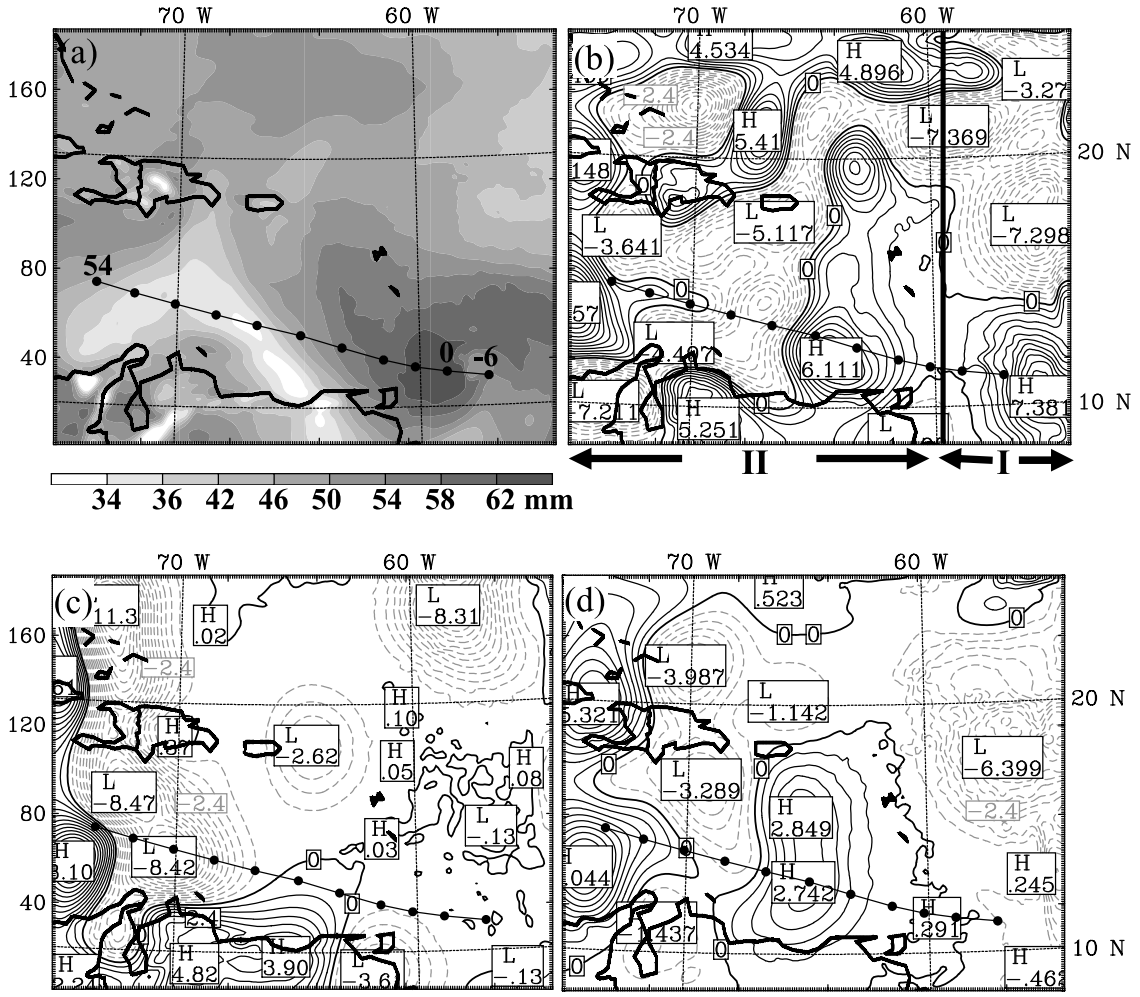

Figure 7. (a) Initial TPW field (mm) in ENONE. Differences (mm) between ENONE and (b) EMI (EMI-ENONE), (c) EMN (EMN-ENONE), and (d) EA (EA-ENONE) at 1800 UTC 13 July 2005 are shown. The contour interval is 0.6 mm, and solid (dotted) lines are positive (negative) values. The zero lines are also shown. Black dots indicate Hurricane Emily's best track position from 1200 UTC July 13 2005 (−6 h) to 0000 UTC 16 July 2005 (54 h), respectively (from east to west). Numerals I and II indicate the areas to the west and to the east of 59°W (denoted by the bold black solid line), respectively.

[23] To statistically examine the impact of the TPW data from MODIS IR, MODIS NIR, and AIRS on Emily's simulations, the mean absolute error (MAE) of the simulated 10 m winds for the four experiments was calculated against the observed 10 m wind from the NOAA Hurricane Research Division. The MAE was averaged inside a 400 km × 400 km domain following the simulated hurricane centers at 14, 20, 26, 32, 38, 44, and 50 h (Figure 5). In addition, the significance levels under the hypothesis that the MAE of 10 m winds from ENONE was larger than those from EMI, EMN, and EA (Table 2) were also examined using a resampling technique [*Wilks*, 1995; *Chien et al.*, 2006; *Chien and Kuo*, 2010]. At 14, 20, 44, and 50 h, the MAEs of ENONE were larger than those of EMI, EMN, and EA with a significance level of at least 78%. MAEs of ENONE were significantly larger than EMI and EMN at 26 h, EMI and EA at 32 h, and EMI at 38 h.

[24] The aforementioned comparisons indicate that when MODIS IR TPW was assimilated, WRF reproduced better simulated track, intensity, and 10 m winds. However, improvement was limited if AIRS TPW or MODIS NIR TPW was used. In certain cases, the simulation results actually became worse.

4.2. Data Impact

4.2.1. Innovation of TPW

[25] The distributions of TPW data coverage from MODIS IR, MODIS NIR, and AIRS and the corresponding innovations (i.e., observation minus the first guess) are shown in Figure 6. Since both MODIS and AIRS are on board the same satellite, Aqua, their coverage areas were very similar, except that the swath of AIRS (1650 km) was narrower than MODIS (2330 km). In addition, the density of MODIS NIR is less than that of MODIS IR because of the data quality control.

[26] Most of the area within MODIS IR swathes had positive innovation. Only small zones of negative innovation were found to the east of and around the Dominican

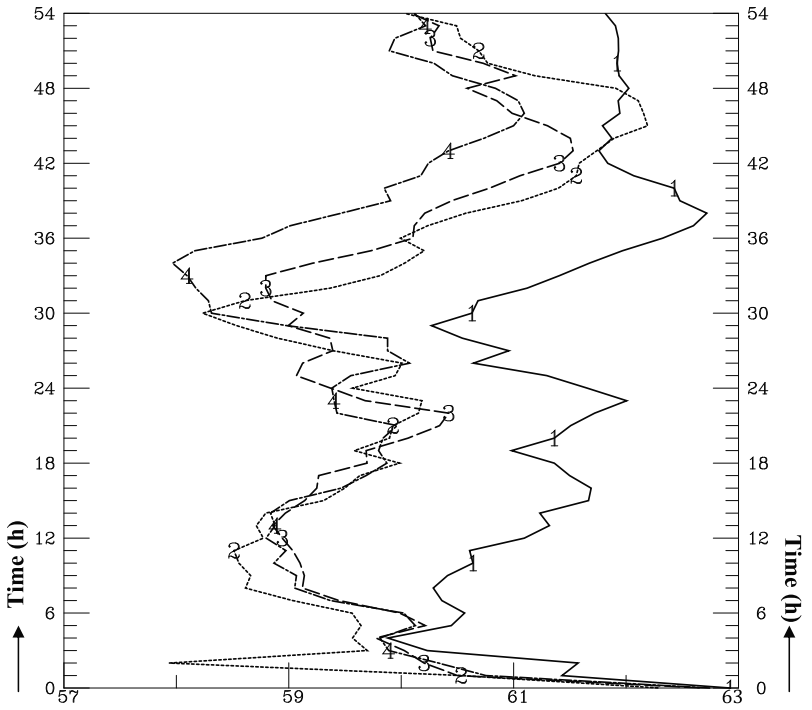

Figure 8. Time series of the TPW averaged inside a 300 km × 300 km box following the center of the simulated hurricane for EMI (1), EMN (2), EA (3), and ENONE (4). The ordinate is time from 0 to 54 h, and the abscissa is TPW in millimeters.

Republic. In contrast, most areas showed negative innovation over MODIS NIR swathes. As for AIRS, positive and negative innovations were equally likely, with positive innovation located to the west and negative innovation located to the east of the observed hurricane. The results of the innovation are consistent with the data characteristics analyzed earlier in the intercomparison. Since MODIS NIR TPW (MODIS IR TPW) was statistically drier (moister) than the others over the ocean, most of its innovation was negative (positive).

4.2.2. Increment of TPW

[27] Figure 7 shows the distribution of the initial TPW field for ENONE and the TPW differences between the other three experiments and ENONE at 1800 UTC 13 July 2005, just after the 6 h data cycling. ENONE showed relatively high TPW around the simulated hurricane, and the atmosphere was relatively dry over the ocean to the north of western Venezuela. The TPW difference between EMI and ENONE ranged from −7.92 to 7.38 mm (Figure 7b). Areas of positive moisture increment were found over the ocean to the north and northeast of eastern Venezuela (Figure 7b, area I) and over the ocean to the north of Colombia (Figure 7b, area II). There was a region of negative increment over the ocean to the north of western Venezuela. For the TPW difference between EMN and ENONE, most areas showed negative values, except in the southwest and the west corners of the domain (Figure 7c). EA was moister than ENONE over area II, but the positive increment was smaller than that between EMI and ENONE around the same location (Figure 7d). EA had a negative increment over area I, which was very different from EMI. The increment pattern of EMI, EMN, and EA in the initial condition was very similar to their innovation pattern, as expected.

[28] To examine how the TPW inside the storm evolved, a domain-averaged TPW within a 300 km × 300 km box following the simulated hurricane centers was computed. Figure 8 presents the time series of the averaged TPW for all experiments. The comparisons showed that at the initial time, the averaged TPWs were very close to each other among the four experiments. The averaged TPW from EMI was larger than the others after a 5 h integration, with a maximum difference of about 2 mm. The TPW magnitudes of EMN, EA, and ENONE were very close to each other before 30 h; after that, ENONE had the smallest averaged TPW, followed by EA and EMN.

4.3. Vertical Wind Shear

[29] Since moisture is an important factor for hurricane intensification, one may expect that the simulated hurricane from EMI should have intensified and become the strongest among all the experiments before 30 h because of its largest TPW within the storm region (Figure 8). However, the hurricane intensity from EMI did not become the strongest until 30 h (Figure 3). This implies that the difference of TPW inside and surrounding the storm among the different experiments might not be the primary trigger of Emily's rapid intensification process.

[30] Many observational and idealized modeling studies have shown the importance of VWS on TC intensity (cited in section 1). To examine how the VWS influenced the simulated intensity of Emily, the horizontal distribution of

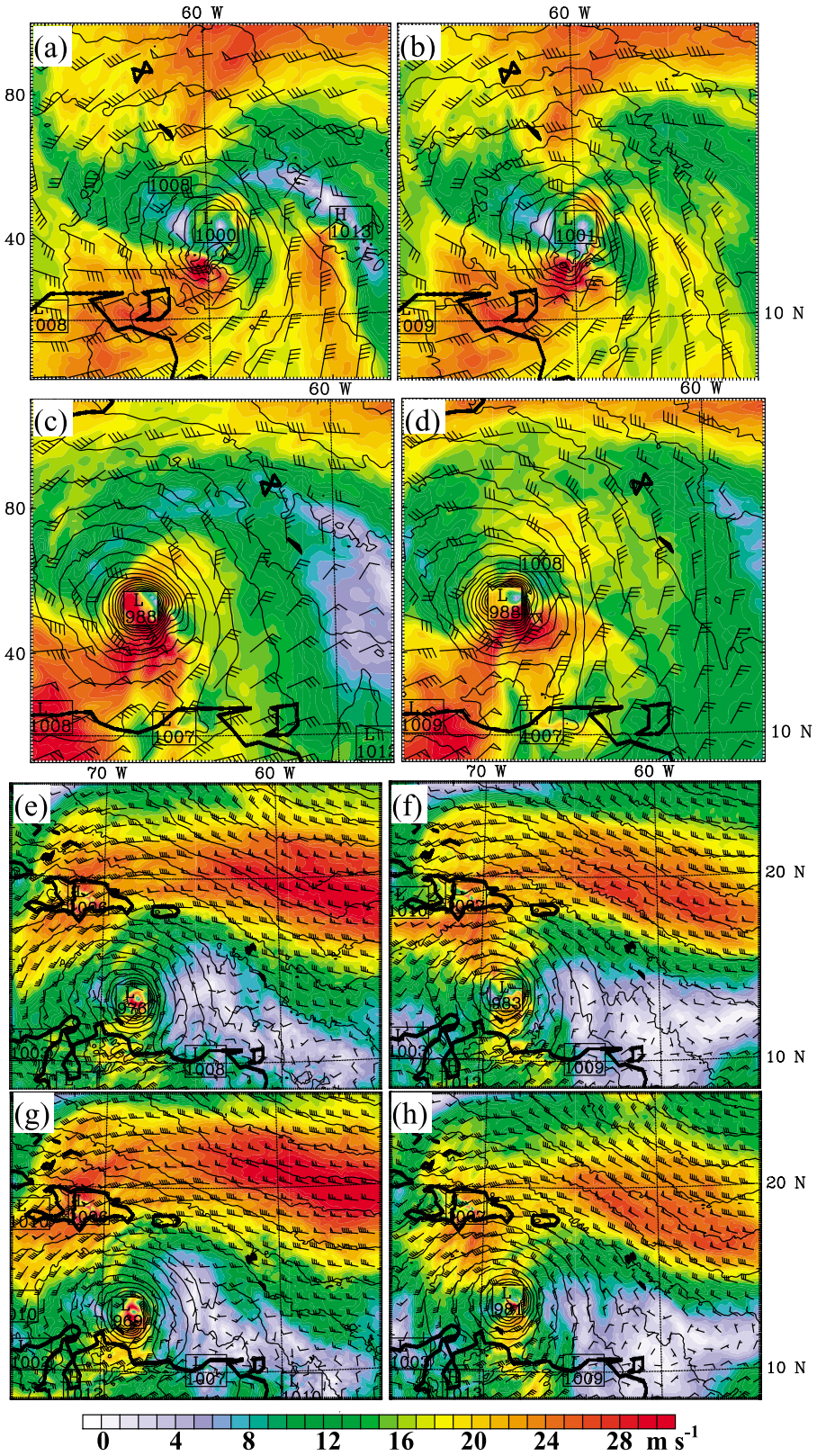

Figure 9. VWS vectors (full barb is 5 m s^{-1}) and magnitude (shaded, m s^{-1}) and sea level pressure (contour, hPa) at (a and b) 4 h, (c and d) 22 h, and (e and f) 34 h for (right) EMI and (right) ENONE, respectively, and at 34 h for (g) ESEN2 and (h) ESEN3, respectively. The bold black solid line is the coastline of Venezuela.

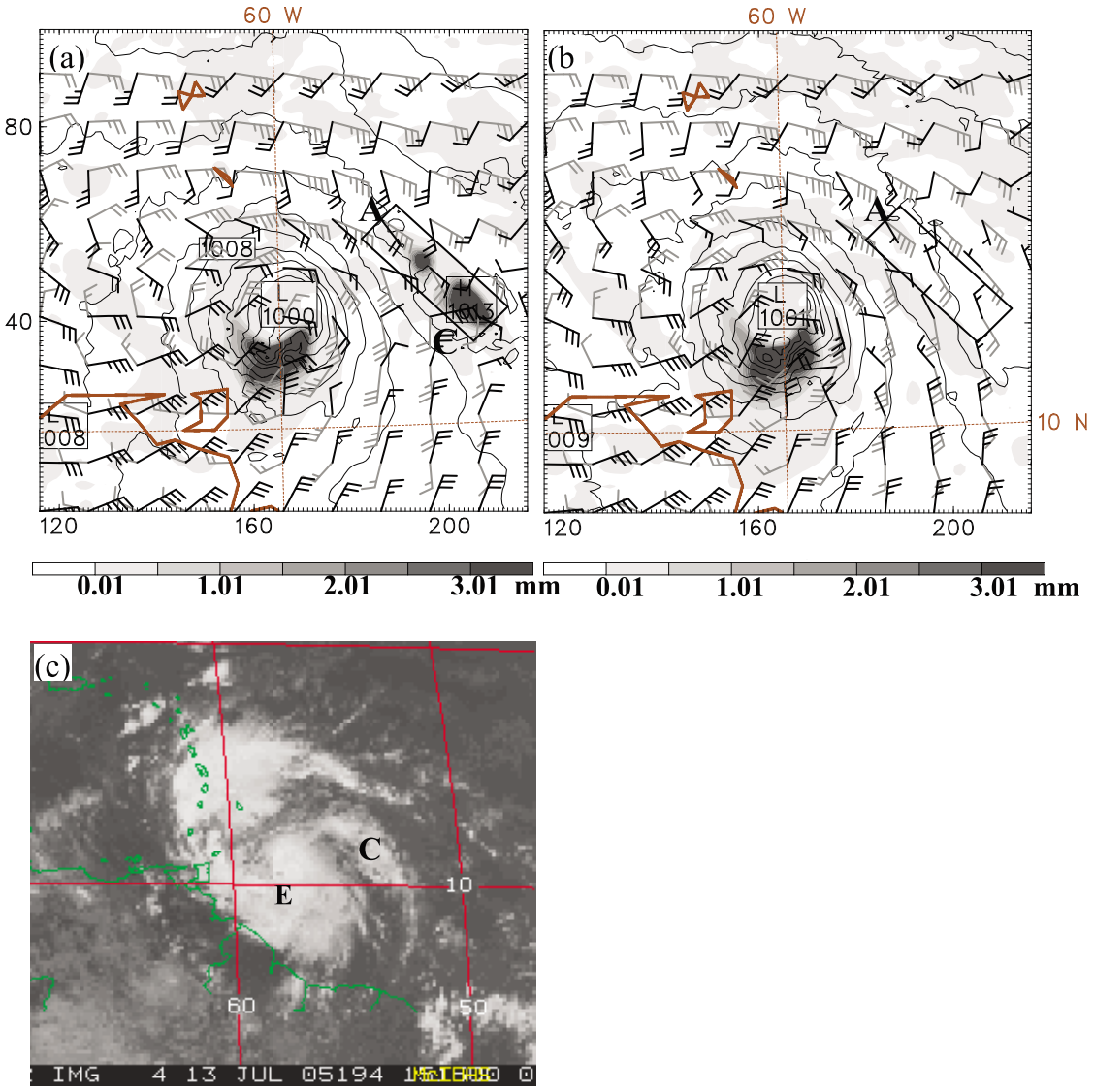

Figure 10. Column-integrated cloud liquid water and precipitation (shaded, mm), sea level pressure (contour lines, hPa), 200 hPa wind vectors in black, and 850 hPa wind vectors in gray (full barb is 5 m s^{-1}) at 5 h for (a) EMI and (b) ENONE. (c) GEOS-12 visible satellite image at 1515 UTC July 13 2005. The letter C indicates a convective cloud, and box A is the area for momentum budget calculations shown in Figure 13. The letter E indicates Hurricane Emily.

VWS vectors and magnitudes from EMI and ENONE at 4, 22, and 34 h are shown in Figures 9a–9f. Because the horizontal distributions of VWSs from EMN, EA, and ENONE were very similar, only the results from ENONE are shown. At the early time, the EMI simulation showed strong shear zones to the north and to the southwest of the storm, and another relatively weaker but still strong shear zone to the southeast of the storm (Figure 9a). The separation of the storm from those strong shear sources might have been the key to Emily's development. Furthermore, a relatively weak VWS band (<7 m s^{-1}, light blue color) was located to the east northeast of the storm. This weak VWS band expanded over time and was advected to the north of the simulated hurricane (Figure 9c), preventing the simulated storm from attaching to the strong shear zone to the north of the storm (in warm colors). Soon after its detachment from the south side of the strong shear zone, the storm started intensifying (Figure 9e). In contrast, the low VWS band did not appear in ENONE early in the simulation (Figure 9b). A relatively large VWS band was found to the east northeast of the storm later on (Figure 9d), which then was advected to the north of the simulated hurricane and attached the storm to the strong shear zone to the north when simulated Emily was detached from the strong shear to the south (Figure 9f). This prevented the storm from rapidly intensifying.

[31] The SLP comparison of the four experiments showed that the minimum SLPs of each run were very close to each other before 24 h (Figure 3). However, after 24 h, the minimum SLP from EMI deepened much more quickly than

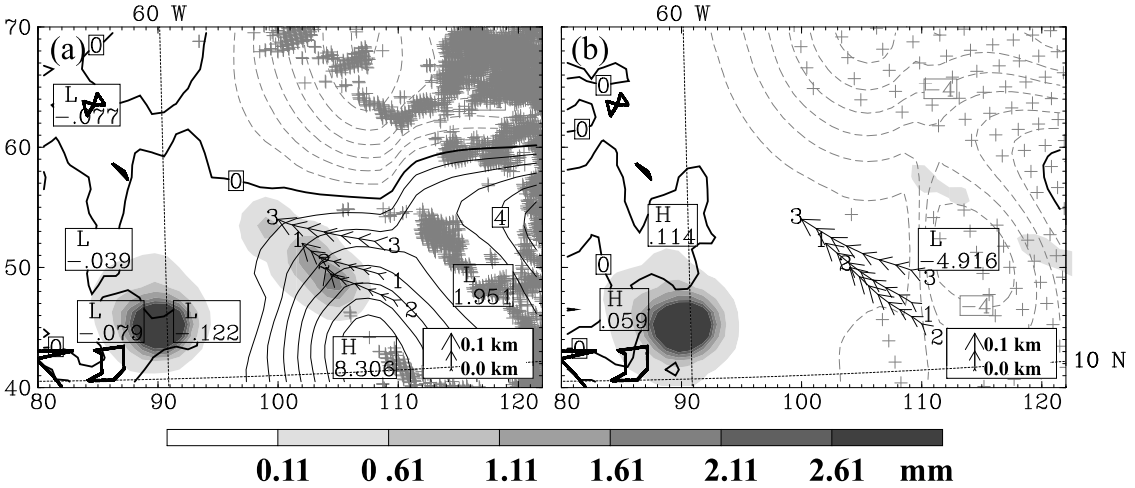

Figure 11. Backward trajectories that were tracked from the 0.1 km height starting at 5 h back to −2 h of the domain 1 simulation. Arrows denote the positions of the air parcels at every hour, and the size indicates the heights of air parcels with the legend shown in the bottom right corner. The increment of (a) MODIS IR TPW and (b) AIRS TPW at −1 h after assimilating the swath of data in the figure (gray plus) and the column-integrated cloud liquid water and precipitation (shaded, mm) at 5 h are also shown.

the others. This strong intensifying period occurred during the time when the weak VWS band in EMI was advected to the north of the simulated hurricane (Figures 9c and 9e) and the simulated storm detached from the strong shear zone to the north. This indicates that the rapid intensification in EMI was highly related to the occurrence of the weak VWS band. As discussed in many hurricane studies (cited in section 1), a large VWS environment is not favorable for TC activity. Therefore the weak VWS band in EMI could serve as a protection zone to separate the storm from the unfavorable large VWS environment between 20°N and 30°N. This is why the hurricane intensified during this time period for EMI, but not the other three experiments.

4.4. Convective Cloud and Trajectory Analysis

[32] An additional analysis was performed to investigate why the assimilation of moisture could modify the VWS to a favorable condition for hurricane development from EMI, but not for the others. Column-integrated hydrometeors show that a convective cloud started to develop to the east northeast of the storm at 1 h (data not shown) and intensified a few hours later (Figure 10a). The convective cloud lasted about 9 h, and its location coincided with the aforementioned weak VWS band (Figure 9a). This convective cloud was also observed in GOES-12 satellite imagery (Figure 10c, C). The evolution of the observed convective cloud was very similar to that from EMI except the cloud in the observation occurred 4 h earlier and lasted 2 h longer than in EMI. In contrast, ENONE, as well as the other experiments, failed to reproduce this convective cloud (Figure 10b).

[33] To trace the origin of the air parcels in the convective cloud area, a backward trajectory was performed (Figure 11). Results showed that the air parcels of convective cloud originated from a region of positive increment in the EMI experiment (Figure 11a) but came from an area of negative increment in the EA experiment (Figure 11b). Therefore, with the moisture-laden air coming into the cloud area in EMI, the convective cloud was successfully reproduced.

4.5. Momentum Budget Analysis

[34] To further examine the role of the convective cloud in producing the weak VWS band, a zoomed-in figure of wind and cloud fields and a 200 hPa momentum budget computed over the area of the convective cloud are shown in Figures 12 and 13, respectively. The 200 and 850 hPa winds inside box A, which covers most of the convective cloud in EMI (Figures 10 and 12), were both southeasterly from ENONE, and the 850 hPa winds were much stronger than the 200 hPa winds at the initial time (Figure 12a). After 2 h, while the 850 hPa winds remained southeasterly but were weaker, the 200 hPa winds started changing direction and turned to north northeasterly at 5 h (Figure 12b), resulting in an increase in VWS in this area. Although the 200 and 850 hPa winds from EMI were similar to those from ENONE at the initial time (Figure 12c), the 200 hPa winds at 5 h from EMI (Figure 12d) were very different from ENONE, and the wind vectors at 200 hPa from EMI were more similar to those at 850 hPa (i.e., a smaller VWS) (Figure 12d).

[35] Figure 13 shows the time evolution of the 200 hPa averaged horizontal momentum budget from 1 to 8 h, which was calculated within box A in Figure 12. The horizontal momentum equations that were adopted here are written as follows:

$$\begin{aligned} \frac{\partial u}{\partial t} &= \left(fv - \frac{1}{\rho}\frac{\partial p}{\partial x}\right) - w\frac{\partial u}{\partial z} - \vec{v_h} \bullet \nabla u + R_x, \\ \frac{\partial v}{\partial t} &= \left(-fu - \frac{1}{\rho}\frac{\partial p}{\partial y}\right) - w\frac{\partial v}{\partial z} - \vec{v_h} \bullet \nabla v + R_y, \end{aligned} \tag{4}$$

where the terms on the left are the local acceleration (first term) and the first four terms on the right are the

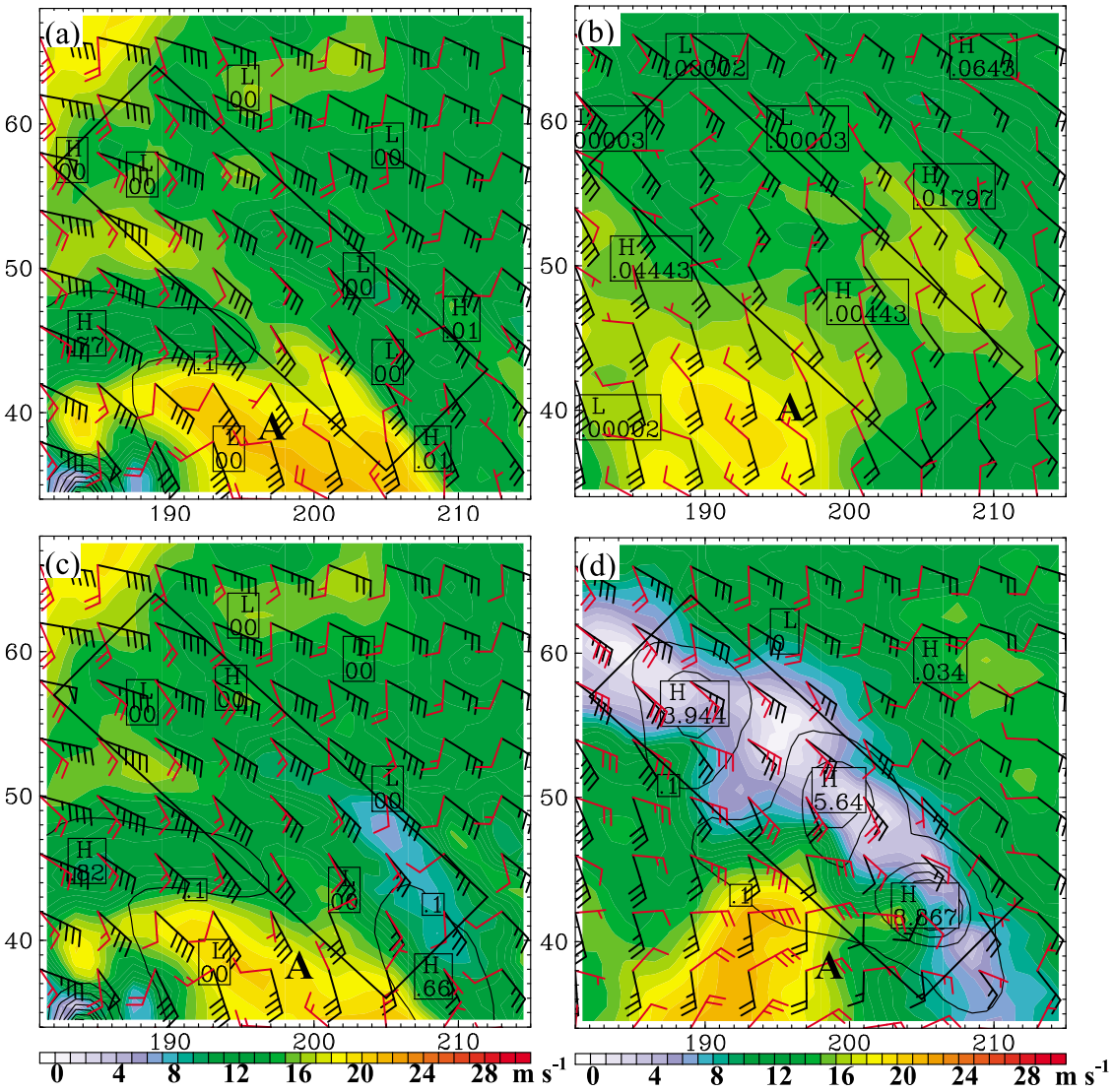

Figure 12. VWS (shaded, m s^{-1}), column-integrated cloud liquid water and precipitation (contour lines, mm), 200 hPa wind barbs in red, and 850 hPa wind barbs in black (full barb is 5 m s^{-1}) at (a) 0 h and (b) 5 h for ENONE and (c) 0 h and (d) 5 h for EMI. Box A is the area for momentum budget calculations shown in Figure 13.

ageostrophic force (i.e., the pressure gradient force plus the coriolis force; second term), vertical advection (third term), horizontal advection (fourth term), and other forcings (fifth term), which account for friction, momentum mixing, and numerical errors.

[36] The southerly wind component, v (curve 6), from ENONE decreased over the plotted period and changed to a northerly wind component after 2 h (Figure 13a). The wind direction change was primarily contributed by the negative ageostrophic force. In contrast, the change of the 200 hPa southerly wind from EMI at the first 3 h (i.e., 1–4 h) was very small because of the cancellation of forces among the positive ageostrophic force and the negative horizontal and vertical advections (Figure 13c). In the next 4 h, the southerly wind component decreased from 6 to 1 m s^{-1}, and the weakening was mainly contributed by the negative vertical advection of v momentum from 4 to 6 h and by the negative ageostrophic force from 6 to 8 h.

[37] The easterly wind speeds (u) and all forcing terms from ENONE were relatively small (Figure 13b). Unlike ENONE, u increased during the first 3 h and remained nearly unchanged afterward from EMI (Figure 13d). The increase in the easterly wind component was mainly contributed by the negative vertical advection of u momentum caused by the cloud-induced upward motion, although it was partially counteracted by the positive ageostrophic force. The increase and decrease of 200 and 850 hPa easterly wind speeds, respectively, made the difference between these two levels smaller, weakening the VWS.

4.6. Sensitivity Studies

[38] After assimilating MODIS IR TPW, two positive moisture increments were located to the east and surrounded

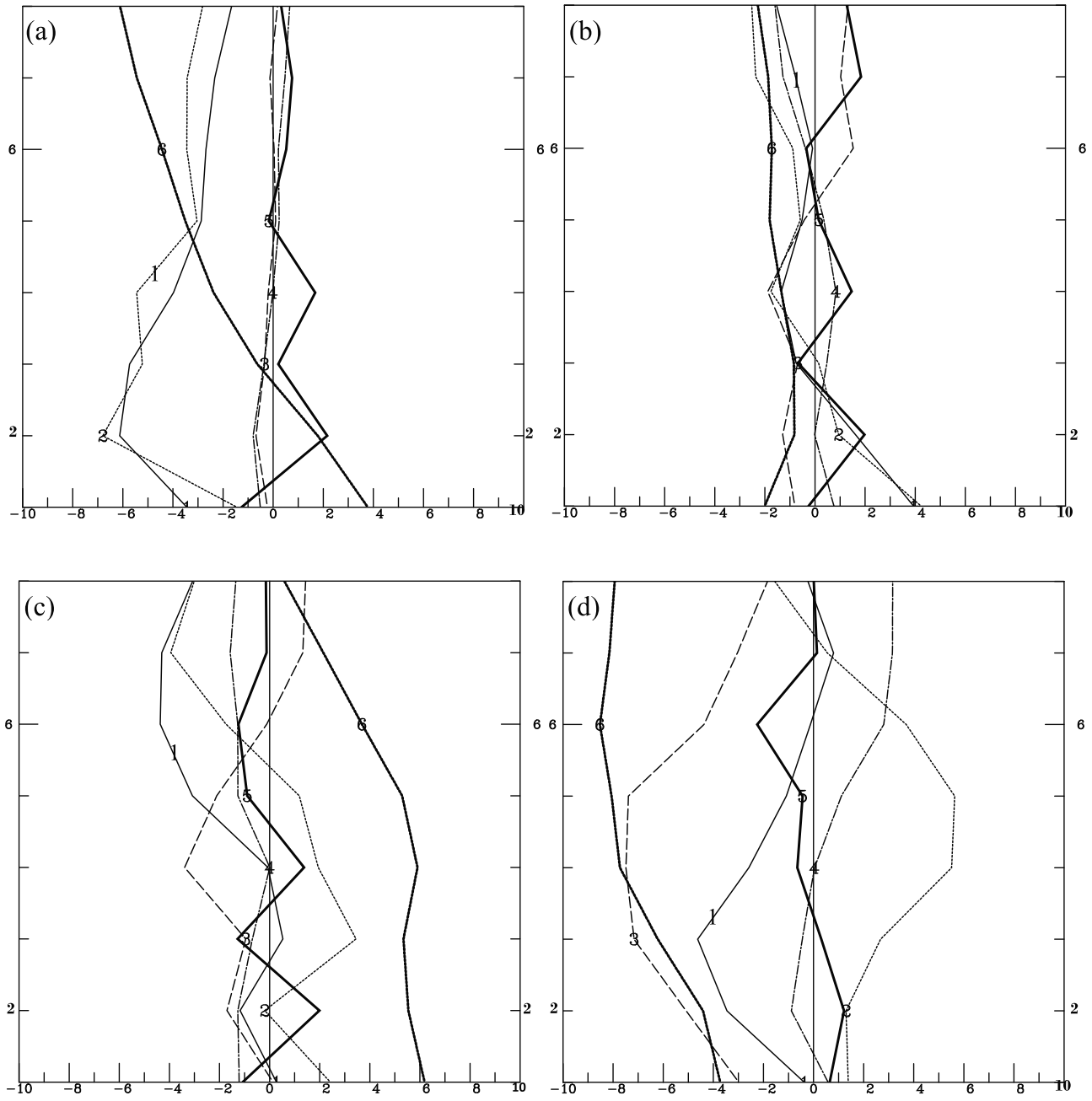

Figure 13. Time series of 200 hPa momentum budget averaged inside box A (shown in Figure 12) for (a and b) ENONE and for (c and d) EMI. The local acceleration (1; $\frac{\partial \vec{u}}{\partial z}$), the ageostrophic force (2; $f\vec{u} - \frac{1}{\rho}\nabla p$), the vertical advection (3; $-w\frac{\partial \vec{u}}{\partial z}$), the horizontal advection (4; $-\vec{v_h} \cdot \nabla \vec{u}$), the residual (5; the residual accounts for friction, momentum mixing, diffusion, etc.), and the wind speeds (6; $\vec{u}$) are transformed into (right) east-west and (left) north-south directions. The ordinate is time from 1 to 8 h, and the abscissa is magnitude in 10^{-4} m s^{-2} for 1–5 and m s^{-1} for 6.

the simulated hurricane at the model initial time (Figure 7b). To further examine the improvement of simulated Emily from EMI, three sensitivity runs were conducted (Table 3). For the first sensitivity experiment (referred to as ESEN1 hereinafter), the initial data at 1800 UTC 13 July 2005, after 6 h update cycling, were the same as those of ENONE except the water vapor mixing ratio was replaced by that from EMI. This will help examine the importance of the moisture increment after the assimilation of MODIS IR TPW. For the second and third sensitivity experiments (referred to as ESEN2 and ESEN3), the initial data were the same as those of EMI except that the water vapor mixing ratios to the west and to the east of 59°W (as shown in Figure 7b), respectively, were replaced by those of ENONE. These two sensitivity studies could help identify the influence of the moisture increment near the convective cloud

Table 3. Sensitivity Experiment Designs for Simulations of Hurricane Emily[a]

Experiment	Data Assimilated
ESEN1	ENONE + q of EMI
ESEN2	EMI + west of 59°W of q of ENONE
ESEN3	EMI + east of 59°W of q of ENONE

[a]ESEN1 indicates the duplicate experiment of ENONE except the water vapor mixing ratio (q) was replaced by that from EMI at 1800 UTC 13 July 2005, after 6 h update cycling. ESEN2 and ESEN3 represent the duplicate simulation of EMI, but q to the west and to the east of 59°W, respectively, were replaced by those from ENONE.

area (Figure 7b, area I) and the simulated hurricane environment (area II) on the intensity change of Emily.

[39] Similar to EMI, the simulated central SLP of the storms from ESEN1 and ESEN2 were significantly intensified after 24 h (Figure 14). In particular, ESEN2 had the largest deepening rate from 24 to 36 h. In contrast, the deepening rate of central pressure from ESEN3 was stronger than ENONE but not as large as the other two sensitivity experiments. This suggests that the positive moisture increment to the east of the storm was important for the rapid intensification of Emily. The horizontal distributions of VWS for ESEN2 and ESEN3 were also examined (Figures 9g and 9h), and they were similar to EMI and ENONE, respectively. Furthermore, ESEN1 and ESEN2 (but not ESEN3) reproduced the deep convective cloud to the east of the storm in the early time of the simulation that was seen in EMI (data not shown).

[40] Results from ESEN1 indicate that the moisture increment from EMI after the assimilation of MODIS IR TPW (Figure 7b) played an important role in the intensification of Emily. Results from ESEN2 and ESEN3 further confirm that the positive TPW increment to the east of the storm at the initial time (Figure 7b, area I), which triggered the convective cloud over the region, was the main reason why the simulated storm intensified from EMI. On the other hand, the positive increment surrounding the storm at the initial time (area II) played a trivial role in intensification.

5. Summary

[41] The impact of MODIS IR, MODIS NIR, and AIRS TPW data on simulations of Hurricane Emily were assessed and compared using the WRF model and its 3D-Var system. After the assimilation of MODIS IR TPW, the model simulation from EMI clearly produced better tracking, intensity, and 10 m wind field of the hurricane than ENONE, which did not assimilate any extra observations. For the EA and EMN experiments, which assimilated AIRS TPW and MODIS NIR TPW, respectively, improvements in the hurricane simulation were limited or nil. The improvement for the EMI simulation may be because, among the three data sets, retrieved MODIS IR TPW statistically tends to be the largest over the ocean, partly fixing the problem of underestimating moisture in the first-guess data.

[42] Although AIRS and MODIS are aboard satellite Aqua, because the swath widths and the retrieved electromagnetic spectrums from both instruments are different (2330 km, IR or NIR channels for MODIS; 1650 km, combined IR and MW channels for AIRS), one could argue that the difference in data coverage could influence data assimilation results. However, after careful examination, we found that the primary reason why Emily from EMI developed was not attributed to the change of the moisture within the core of the hurricane but to the reproduction of the convective cloud to the east of the hurricane. After the assimilation of MODIS IR TPW, a positive moisture increment was present to the east of the simulated storm in

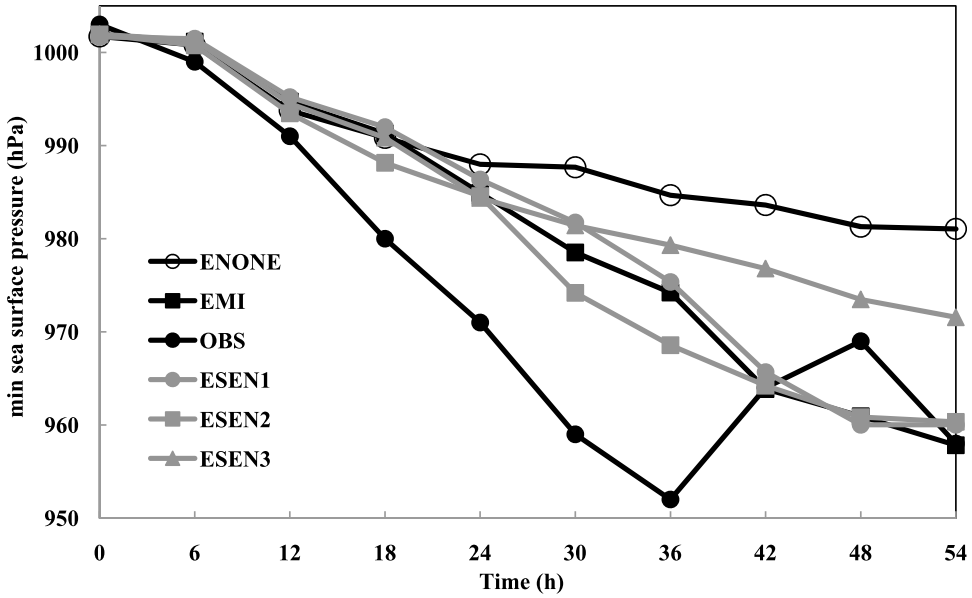

Figure 14. Time series of the observed central SLP from the best-track (OBS) and the simulated central SLP (hPa) from ENONE, EMI, ESEN1, ESEN2, and ESEN3 from 1800 UTC 13 July to 0000 UTC 16 July 2005.

the 3D-Var analysis (i.e., initial conditions). The positive TPW anomaly helped produce a convective cloud (as seen in the analysis of the backward trajectory), a key player in the rapid intensification, which was also observed by satellites. The convective cloud effectively transported momentum upward (shown by analysis of the momentum budget) and modulated the height field, reducing the difference between horizontal winds in lower and upper levels, and thus resulted in the weakening of VWS over the region. The weak VWS band was advected to the north of the storm, detaching the storm from the strong VWS zone located between 20°N and 30°N. This greatly helped the intensification of Hurricane Emily. Three sensitivity experiments were conducted to further confirm the role of the convective cloud in Emily's intensification.

[43] On the other hand, after assimilating either MODIS NIR or AIRS TPW, there was no such positive moisture increment to the east of the simulated storm. Thus EMN and EA, as well as ENONE, failed to reproduce this convective cloud. As a result, a relatively larger VWS band was located to the east northeast of the storm. The large VWS band propagated to the north of the simulated hurricane and attached the storm to the strong shear zone, preventing the storm from developing.

[44] This study demonstrates a new mechanism by which a convective cloud helps TC intensification in an early stage under a strong shear environment. For simulated Emily from EMI, the convective cloud to the northeast of the TC could effectively transport momentum upward through the upward motion and result in a weak VWS band, which served as a protection zone to separate the storm from the unfavorable large VWS environment between 20°N and 30°N, and, in consequence, the storm developed. However, this mechanism is based only on one case study, and more case studies, including the use of observations, will be required to further clarify the importance of the proposed mechanism through which convective clouds influence hurricane intensification.

[45] **Acknowledgments.** We acknowledge the WRF model and WRF-VAR development teams for their efforts on model development. We also thank Cheng-Shang Lee (National Taiwan University (NTU)) for helpful comments, Ke Chen (North Carolina State University) and Wei-Ting Fang (NTU) for help with Matlab graphs, and John Chiu and Rex Chen for proofreading the manuscript. The MODIS data were obtained from the NASA Goddard Space Flight Center. The AIRS data were obtained from the NASA Jet Propulsion Laboratory. This work was supported by NASA grants NNG04GM90G 521 NRA 03-OES-02 and NNX09AC38G (Hurricane Science Research Program) and was also partly supported by National Science Council of Taiwan grant NSC 97-2111-M-003-002-MY2.

References

Aiyyer, A. R., and C. Thorncroft (2006), Climatology of vertical wind shear over the tropical Atlantic, *J. Clim.*, *19*, 2969–2983, doi:10.1175/JCLI3685.1.

Beven, J. L., II, L. A. Avila, E. S. Blake, D. P. Brown, J. L. Franklin, R. D. Knabb, R. J. Pasch, J. R. Rhome, and S. R. Stewart (2008), Atlantic hurricane season of 2005, *Mon. Weather Rev.*, *136*, 1109–1173, doi:10.1175/2007MWR2074.1.

Black, M. L., J. E. Gamache, F. D. Marks Jr., C. E. Samsury, and H. E. Willoughby (2002), Eastern Pacific hurricanes Jimena of 1991 and Olivia of 1994: The effect of vertical shear on structure and intensity, *Mon. Weather Rev.*, *130*, 2291–2312, doi:10.1175/1520-0493(2002)130<2291:EPHJOA>2.0.CO;2.

Bracken, W. E., and L. F. Bosart (2000), The role of synoptic-scale flow during tropical cyclogenesis over the North Atlantic Ocean, *Mon. Weather Rev.*, *128*, 353–376, doi:10.1175/1520-0493(2000)128<0353:TROSSF>2.0.CO;2.

Burpee, R. W., and M. L. Black (1989), Temporal and spatial variations of rainfall near the centers of two tropical cyclones, *Mon. Weather Rev.*, *117*, 2204–2218, doi:10.1175/1520-0493(1989)117<2204:TASVOR>2.0.CO;2.

Cecil, D. J., K. R. Quinlan, and D. M. Mach (2010), Intense convection observed by NASA ER-2 in Hurricane Emily (2005), *Mon. Weather Rev.*, *138*, 765–780, doi:10.1175/2009MWR3063.1.

Chen, S. H., and W.-Y. Sun (2002), A one-dimensional time-dependent cloud model, *J. Meteorol. Soc. Jpn.*, *80*, 99–118, doi:10.2151/jmsj.80.99.

Chen, S. H., Z. Zhao, J. S. Haase, A. Chen, and F. Vandenberghe (2008), A study of the characteristics and assimilation of retrieved MODIS total precipitable water data in severe weather simulations, *Mon. Weather Rev.*, *136*, 3608–3628, doi:10.1175/2008MWR2384.1.

Chien, F.-C., and Y.-H. Kuo (2010), Impact of FORMOSAT-3/COSMIC GPS radio occultation and dropwindsonde data on regional model predictions during the 2007 Mei-yu season, *GPS Solut.*, *14*, 51–63, doi:10.1007/s10291-009-0143-2.

Chien, F.-C., Y.-C. Liu, and B. J.-D. Jou (2006), MM5 ensemble mean forecasts in the Taiwan area for the 2003 Mei-yu season, *Weather Forecast.*, *21*, 1006–1023, doi:10.1175/WAF960.1.

DeMaria, M. (1996), The effect of vertical shear on tropical cyclone intensity change, *J. Atmos. Sci.*, *53*, 2076–2088, doi:10.1175/1520-0469(1996)053<2076:TEOVSO>2.0.CO;2.

Dudhia, J. (1989), Numerical study of convection observed during the winter monsoon experiment using a mesoscale two-dimensional model, *J. Atmos. Sci.*, *46*, 3077–3107, doi:10.1175/1520-0469(1989)046<3077:NSOCOD>2.0.CO;2.

Frank, W. M. (1977), The structure and energetics of the tropical cyclone: part I. Storm structure, *Mon. Weather Rev.*, *105*, 1119–1135, doi:10.1175/1520-0493(1977)105<1119:TSAEOT>2.0.CO;2.

Frank, W. M., and E. A. Ritchie (2001), Effects of vertical wind shear on the intensity and structure of numerically simulated hurricanes, *Mon. Weather Rev.*, *129*, 2249–2269, doi:10.1175/1520-0493(2001)129<2249:EOVWSO>2.0.CO;2.

Franklin, J. L., S. J. Lord, S. E. Feuer, and F. D. Marks Jr. (1993), The kinematic structure of Hurricane Gloria (1985) determined from nested analyses of dropwindsondes and Doppler radar data, *Mon. Weather Rev.*, *121*, 2433–2451, doi:10.1175/1520-0493(1993)121<2433:TKSOHG>2.0.CO;2.

Gao, B.-C., and Y. J. Kaufman (2003), Water vapor retrievals using Moderate Resolution Imaging Spectroradiometer (MODIS) near-infrared channels, *J. Geophys. Res.*, *108*(D13), 4389, doi:10.1029/2002JD003023.

Gentry, M. S., and G. M. Lackmann (2010), Sensitivity of simulated tropical cyclone structure and intensity to horizontal resolution, *Mon. Weather Rev.*, *138*, 688–704, doi:10.1175/2009MWR2976.1.

Gray, W. M. (1968), Global view of the origin of tropical disturbances and storms, *Mon. Weather Rev.*, *96*, 669–700, doi:10.1175/1520-0493(1968)096<0669:GVOTOO>2.0.CO;2.

Hong, S.-Y., Y. Noh, and J. Dudhia (2006), A new vertical diffusion package with an explicit treatment of entrainment processes, *Mon. Weather Rev.*, *134*, 2318–2341, doi:10.1175/MWR3199.1.

Jones, S. C. (2000), The evolution of vortices in vertical shear: III. Baroclinic vortices, *Q. J. R. Meteorol. Soc.*, *126*, 3161–3185, doi:10.1002/qj.49712657009.

Kain, J. S. (2004), The Kain-Fritsch convective parameterization: An update, *J. Appl. Meteorol.*, *43*, 170–181, doi:10.1175/1520-0450(2004)043<0170:TKCPAU>2.0.CO;2.

Kalnay, E. (2003), *Atmospheric Modeling, Data Assimilation and Predictability*, 341 pp., Cambridge Univ. Press, Cambridge, U. K.

Kleidman, R. G., Y. J. Kaufman, B.-C. Gao, L. A. Remer, V. G. Brackett, R. A. Ferrare, E. V. Browell, and S. Ismail (2000), Remote sensing of total precipitable water vapor in the near-IR over ocean glint, *Geophys. Res. Lett.*, *27*, 2657–2660, doi:10.1029/1999GL011156.

Li, X., and Z. Pu (2008), Sensitivity of numerical simulation of early rapid intensification of Hurricane Emily (2005) to cloud microphysical and planetary boundary layer parameterizations, *Mon. Weather Rev.*, *136*, 4819–4838, doi:10.1175/2008MWR2366.1.

Li, X., and Z. Pu (2009), Sensitivity of numerical simulations of the early rapid intensification of Hurricane Emily (2005) to cumulus parameterization schemes in different model grid resolutions, *J. Meteorol. Soc. Jpn.*, *87*, 403–421.

Marks, F. D., Jr., R. A. Houze Jr., and J. F. Gamache (1992), Dual-aircraft investigation of the inner core of Hurricane Norbert: part I. Kinematic structure, *J. Atmos. Sci.*, *49*, 919–942, doi:10.1175/1520-0469(1992)049<0919:DAIOTI>2.0.CO;2.

Miller, B. L. (1958), Rainfall rates in Florida hurricanes, *Mon. Weather Rev.*, *86*, 258–264, doi:10.1175/1520-0493(1958)086<0258:RRIFH>2.0.CO;2.

Mlawer, E. J., S. J. Taubman, P. D. Brown, M. J. Iacono, and S. A. Clough (1997), Radiative transfer for inhomogeneous atmosphere: RRTM, a validated correlated-k model for the long-wave, *J. Geophys. Res.*, *102*, 16,663–16,682, doi:10.1029/97JD00237.

Nolan, D. S., D. P. Stern, and J. A. Zhang (2009), Evaluation of planetary boundary layer parameterizations in tropical cyclones by comparison of in situ observations and high-resolution simulations of Hurricane Isabel (2003): part II. Inner-core boundary layer and eyewall structure, *Mon. Weather Rev.*, *137*, 3675–3698, doi:10.1175/2009MWR2786.1.

Pu, Z., X. Li, and E. J. Zipse (2009), Diagnosis of the initial and forecast errors in the numerical simulation of the rapid intensification of Hurricane Emily (2005), *Weather Forecast.*, *24*, 1236–1251, doi:10.1175/2009WAF2222195.1.

Rama Varma Raja, M. K., S. I. Gutman, J. G. Yoe, L. M. Mcmillin, and J. Zhao (2008), The validation of AIRS retrievals of integrated precipitable water vapor using measurements from a network of ground-based GPS receivers over the contiguous United States, *J. Atmos. Oceanic Technol.*, *25*, 416–428, doi:10.1175/2007JTECHA889.1.

Seemann, S. W., J. Li, W. P. Menzel, and L. E. Gumley (2003), Operational retrieval of atmospheric temperature, moisture, and ozone from MODIS infrared radiances, *J. Appl. Meteorol.*, *42*, 1072–1091, doi:10.1175/1520-0450(2003)042<1072:OROATM>2.0.CO;2.

Skamarock, W. C., J. B. Klemp, J. Dudhia, D. O. Gill, D. M. Barker, M. G. Duda, X.-Y. Huang, W. Wang, and J. G. Powers (2008), A description of the advanced research WRF version 3, *Tech. Note NCAR/TN-475+STR*, 125 pp., Natl. Cent. for Atmos. Res., Boulder, Colo.

Strow, L. L., S. E. Hannon, S. De-Souza Machado, H. E. Motteler, and D. C. Tobin (2006), Validation of the Atmospheric Infrared Sounder radiative transfer algorithm, *J. Geophys. Res.*, *111*, D09S06, doi:10.1029/2005JD006146.

Wang, Y., and G. J. Holland (1996), Tropical cyclone motion and evolution in vertical shear, *J. Atmos. Sci.*, *53*, 3313–3332, doi:10.1175/1520-0469(1996)053<3313:TCMAEI>2.0.CO;2.

Wilks, D. S. (1995), *Statistical Methods in the Atmospheric Sciences*, 467 pp., Academic, San Diego, Calif.

Zehr, R. M. (1992), Tropical cyclogenesis in the western north Pacific, *NOAA Tech. Rep. NESDIS 61*, 181 pp., NOAA Natl. Environ. Satellite, Data, and Inf. Serv., Washington, D. C.

Zhang, X., Q. Xiao, and P. Fitzpatrick (2007), The impact of multisatellite data on the initialization and simulation of Hurricane Lili's (2002) rapid weakening phase, *Mon. Weather Rev.*, *135*, 526–548, doi:10.1175/MWR3287.1.

Zhu, T., D.-L. Zhang, and F. Weng (2004), Numerical simulation of Hurricane Bonnie (1998): part I. Eyewall evolution and intensity changes, *Mon. Weather Rev.*, *132*, 225–241, doi:10.1175/1520-0493(2004)132<0225:NSOHBP>2.0.CO;2.

S.-H. Chen and Y.-C. Liu, Department of Land, Air, and Water Resources, University of California, One Shields Avenue, Davis, CA 95616-8627, USA. (shachen@ucdavis.edu)

F.-C. Chien, Department of Earth Sciences, National Taiwan Normal University, No. 88, Sec. 4, Tingzhou Rd., Wenshan District, Taipei 11677, Taiwan.